Langmuir Article

pubs.acs.org/Langmuir

Nanoscale Wetting on Groove-Patterned Surfaces

Xin Yong and Lucy T. Zhang*

Department of Mechanical, Aerospace, and Nuclear Engineering, Rensselaer Polytechnic Institute, 110 Eighth Street, Troy, New York 12180

Received December 6, 2008. Revised Manuscript Received February 17, 2009

In this paper, nanoscale wetting on groove-patterned surfaces is thoroughly studied using molecular dynamics simulations. The results are compared with Wenzel's and Cassie's predictions to determine whether these continuum theories are still valid at the nanoscale for both hydrophobic and hydrophilic types of surfaces when the droplet size is comparable to the groove size. A system with a liquid mercury droplet and grooved copper substrate is simulated. The wetting properties are determined by measuring contact angles of the liquid droplet at equilibrium states. Correlations are established between the contact angle, roughness factor r, and surface fraction f. The results show that, for hydrophobic surfaces, the contact angle as a function of roughness factor and surface fraction on nanogrooved surfaces obeys the predictions from Wenzel's theory for wetted contacts and Cassie's theory for composite contacts. However, slight deviations occur in composite contacts when a small amount of liquid penetration is observed. The contact angle of this partial wetting cannot be accurately predicted using either Cassie's or Wenzel's theories. For hydrophilic surfaces, only wetted contacts are observed. In most cases, the resulting contact angles are found to be higher than Wenzel's predictions. At the nanoscale, high surface edge density plays an important role, which results in contact line pinning near plateau edges. For both hydrophobic and hydrophilic surfaces, substantial amount of anistropic spreading is found in the direction that is parallel to the grooves, especially at wetted or partially wetted contacts.

1. Introduction

The fascinating features and properties of interfacial hydrodynamics of interacting liquids and solids inspired numerous designs of material surfaces that can capture and facilitate desired functions. The well-known "lotus effect" that denotes roughness-induced superhydrophobicity and self-cleaning abilities of biological and artificial surfaces has been adopted in various applications in many disciplines. Both experimental and computational investigations[1−6] have been extensively applied to this subject for decades. A notable application is designing self-cleaning mechanisms that can detect and remove hazard particles as the liquid droplet rolls away.[5,7,8] With increasing interests in miniaturized designs of nano- and microfluidic systems and devices, scientists are able to obtain desired wetting properties for specific applications that do not operate at the macroscale. The theory of wetting that had been established at the macroscale is no longer valid, as the liquid may be more sensitive to the surface structure and chemistry.

Numerical studies[9] have been done in attempts to understand the wetting properties on micropatterned surfaces. The results show that static wetting properties such as the contact angle do not exhibit major deviations comparing with the ones obtained at the macroscale. On the experimental side, Extrand[10] measured contact angle and hysteresis on surfaces with chemically heterogeneous islands and Gao and McCarthy's experiments[11] examined the contact angle behavior on three types of two-component surfaces. Both of these experimental findings question the validity of Wenzel's and Cassie's theories.

At the nanoscale, researchers have used molecular dynamics and Monte Carlo simulations to study nanowetting properties of liquid droplets and their interfaces with distinct solid surfaces.[12−22] The validity of continuum theories for geometrically patterned hydrophobic surfaces at the nanoscale was studied by Hirvi and Pakkanen.[23] A series of work was reported to investigate the wetting of a water droplet on 1-D ordering nanogrooved PE and PVC polymer hydrophobic surfaces. The contact angles obtained at the equilibrium states with composite contacts were in good agreement with predictions from Cassie's theory. However, for relatively smooth surfaces that result in wetted contacts, they found that Wenzel's theory overestimates the contact angles. The validities of Young's equation and Cassie's

*To whom correspondence should be addressed. E-mail: zhangLucy@rpi.edu. Telephone: (518) 276-6914. Fax: (518) 276-2623.

(1) de Gennes, P. *Rev. Mod. Phys.* **1985**, *57*, 827–863.
(2) Shibuichi, S.; Onda, T.; Satoh, N.; Tsujii, K. *J. Chem. Phys.* **1996**, *100*, 19512–19517.
(3) Mahadevan, L.; Pomeau, Y. *Phys. Fluids* **1999**, *11*, 2449–2453.
(4) McGaughey, A. J.; Ward, C. *J. Appl. Phys.* **2003**, *93*, 3619–3626.
(5) Marmur, A. *Langmuir* **2004**, *20*, 3517–3519.
(6) Suzuki, T.; Hirose, G.; Oishi, S. *Mater. Res. Bull.* **2004**, *39*, 103–108.
(7) Barthlott, W.; Neinhuis, C. *Planta* **1997**, *202*, 1–8.
(8) Neinhuis, C.; Barthlott, W. *Ann. Bot.* **1997**, *79*, 667–677.
(9) Patakar, N. A.; Chen, Y. Numerical simulation of droplet shapes on rough surfaces. *Modeling and Simulation of Microsystems*, Nanotech 2002 Vol. 1 Technical Proceedings of the 2002 International Conference on Modeling and Simulation of Microsystems; MSM 2002, April 21-25, 2002, San Jaun, Puerto Rico; Computational Publications: Cambridge, MA, 2002.
(10) Extrand, C. *Langmuir* **2003**, *19*, 3793–3796.
(11) Gao, L.; McCarthy, T. J. *Langmuir* **2007**, *23*, 3762–3765.
(12) Sikkenk, J.; Indekeu, J.; van Leeuwen, J. *Phys. Rev. Lett.* **1987**, *59*, 98–101.
(13) Schlick, T.; Figueroa, S. *J. Chem. Phys.* **1991**, *94*, 2118–2129.
(14) Lundgren, M.; Allan, N. L.; Cosgrove, T. *Langmuir* **2002**, *18*, 10462–10466.
(15) Kim, J.; Kim, C.-J. C. *Nanostructured surfaces for dramatic reduction of flow resistance in droplet-based microfluidics*. The Fifteenth IEEE International Conference on Micro Electro Mechanical Systems, Las Vegas, Nevada, January 20-24, 2002; IEEE: Piscataway, NJ, 2002.
(16) Yaneva, J.; Milchev, A.; Binder, K. *Macromol. Theory Simul.* **2003**, *12*, 573–581.
(17) Werder, T.; Walther, J.; Jaffe, R.; Halicioglu, T.; Koumoutsakos, P. *J. Phys. Chem. B* **2003**, *107*, 1345–1352.
(18) Schneemilch, M.; Quirke, N.; Henderson, J. *J. Chem. Phys.* **2004**, *120*, 2901–2912.
(19) Voronov, R. S.; Papavassiliou, D. V.; Lee, L. L. *J. Chem. Phys.* **2006**, *124*, 204701.
(20) Hirvi, J. T.; Pakkanen, T. A. *J. Chem. Phys.* **2006**, *125*, 144712.
(21) Ingebrigtsen, T.; Texvaerd, S. *J. Phys. Chem. C* **2007**, *111*, 8518–8523.
(22) Seemann, R.; Brinkmann, M.; Karmer, E. J.; Lange, F. F.; Lipowsky, R. *Proc. Natl. Acad. Sci. U.S.A.* **2005**, *102*, 1848–1852.
(23) Hirvi, J. T.; Pakkanen, T. A. *Langmuir* **2007**, *23*, 7724–7729.

theory at the nanoscale were also examined by Schneemilch and his colleagues through numerical simulations of chemically patterned surfaces. They performed studies on wetting of small saturated liquid−vapor coexistent system on chemically treated surfaces with striped and hexagonal disk patterns.[18,24] The wetting properties were studied by applying high chemical contrast between the patches and background surfaces. They found that both Young's equation and Cassie's theories are only valid when the interactions between the liquid and the substrate are relatively weak. A more detailed description can be found in their publications. Besides chemically and mechanically treating a substrate surface, the size of the droplet in comparison with the size of the patterns on a substrate can also play an important role at the nanoscale. In the report by Lundgren et al.,[25] they reported that Cassie's theory breaks down when the size of the patterns on a heterogeneous surface is comparable to or larger than the droplet radius. They further performed studies on hydrophobic pillar surfaces and they found that both Wenzel's and Cassie's theories again break down as soon as the pattern size becomes comparable or larger than the droplet size. Seemann et al.[22] reported both experimental and simulation results of different liquid wetting morphologies on groove-patterned surfaces with rectangular cross sections. In all the studies with 1-D geometrically or chemically patterned surfaces, strong anisotropic liquid spreading is observed, as explained in Hirvi and Pakkanen.[23] Xia and Brueck[26] confirmed this observation by experimentally studying a microscopic water droplet on both hydrophobic and hydrophilic 1-D nanopatterned surfaces.

The aforementioned research results have shown that there are several factors in determining the validity of Wenzel's and Cassie's theories. In this paper, we intend to use molecular dynamics to thoroughly perform a series of studies on the wetting behavior of droplets on nanogrooved surfaces, in particular, the relationships of the contact angle with roughness factor and surface fraction. We will examine both intrinsically hydrophobic and hydrophilic surfaces and focus our results on the cases when the droplet size is comparable to the groove size. A series of simulations are designed to investigate the validity of Wenzel's and Cassie's theories at the nanoscale by varying the design parameters of the grooves. Anisotropic spreading of the liquid droplet will also be discussed.

An outline of the paper is as follows. We will first describe the details of the simulation method and models in section 2. We will also perform a calibration study to represent the hydrophobic and hydrophilic surfaces by adjusting the relative energy parameter (section 2.5). The results will be presented and discussed in section 3 for both hydrophobic and hydrophilic surfaces. Finally, the conclusions will be drawn in section 4.

2. Simulation Method and Models

In this section, we will first review the wetting theories that are used at the macroscale: Wenzel's and Cassie's theories, which are built based on the Young's equation. Then, we will discuss in detail the simulation method and models, which include the interatomic potential and parameters, model systems, contact angle calculation, and surface hydrophobicity calibration.

2.1. Theories. The mechanical contact angle, θ_e, that a liquid droplet forms on an ideal flat surface was first described by Young's equation.[27] It relates the contact angle with the surface tensions of three interfaces as

$$\gamma_{lv} \cos \theta_e = \gamma_{sl} - \gamma_{sv} \quad (1)$$

where s, l, and v represent solid, liquid, and vapor, respectively. There are three major factors that govern the wettability of a surface: its intrinsic surface energy, surface roughness, and surface homogeneity. In static wettings, a geometrically patterned surface, for example, grooved surface, results in two types of contacts: wetted contact (Wenzel state) and composite contact (Cassie state). A wetted contact is where the liquid penetrates into the grooves and wets the solid substrate (Figure 1, left), while a composite contact is where air is trapped in the grooves and the liquid sits on the plateau of the surface without any penetration (Figure 1, right).

The contact angle of a wetted contact on a rough surface is best described using Wenzel's theory, which predicts the contact angle as a result of the surface roughness based on the modification of the Young's equation. The apparent Wenzel's contact angle, θ^W, can be calculated as

$$\cos \theta^W = r \cos \theta_e \quad (2)$$

where r is the roughness factor, defined as the ratio of the true area of the solid surface to its projected area. According to this equation, the wettability of a surface depends on its roughness factor and the intrinsic contact angle on a smooth surface θ_e. On a hydrophilic surface ($\theta_e < 90°$), surface roughness increases the wettability by absorbing the liquid into the grooves. However, on a hydrophobic surface ($\theta_e > 90°$), the roughness can decrease the wettability because it gets energetically too expensive for the liquid to sink into the grooves and wet the groove surface. Therefore, surface roughness can lower wettability and induce high hydrophobicity or superhydrophobicity on a hydrophobic surface and increase wettability on a hydrophilic surface.[28]

The contact angle of a composite contact is described using Cassie's theory which relates the apparent Cassie's contact angle, θ^C, with the composition of the surface. For a heterogeneous surface that is composed of two materials, it is

$$\cos \theta^C = f_A \cos \theta_e^A + f_B \cos \theta_e^B \quad (3)$$

in which f_A and f_B are the fractions of the two components; θ_e^A and θ_e^B are the intrinsic contact angles on smooth surfaces A and B, respectively. For a composite contact, the surface is considered as having two distinct components, substrate and air, because air is trapped in the grooves. Equation 3 can then be written as

$$\cos \theta^C = f \cos \theta_e - (1 - f) \quad (4)$$

where f and $1 - f$ represent the surface fraction of the liquid−solid and liquid−air interfaces, respectively. According to this equation, a composite contact can also result in an increase in hydrophobicity.

When the total energy in a system is minimized, the system reaches an equilibrium state with either wetted contact or composite contact depending on which one requires a lower energy. To predict the equilibrium contact states mathematically, we first find a critical contact angle $\theta_e^{W=C}$ by equating eqs 2 and 4 as shown in Patankar:[28]

$$\theta_e^{W=C} = \cos^{-1}\left(\frac{1-f}{f-r}\right) \quad (5)$$

(24) Schneemilch, M.; Quirke, N.; Henderson, J. *J. Chem. Phys.* **2003**, *118*, 816–829.
(25) Lundgren, M.; Allan, N. L.; Cosgrove, T. *Langmuir* **2007**, *23*, 1187–1194.
(26) Xia, D.; Brueck, S. *Nano Lett.* **2008**, *8*, 2819–2824.
(27) Young, T. *Philos. Trans. R. Soc. London* **1805**, *95*, 65–87.
(28) Patankar, N. A. *Langmuir* **2003**, *19*, 1249–1253.

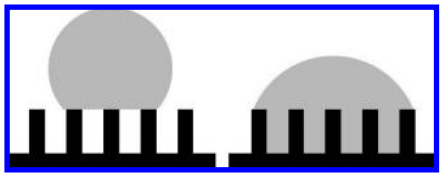

Figure 1. Schematic illustrations of (left) a composite contact and (right) a wetted contact.

Theoretically, this critical contact angle sets apart a wetted contact from a composite contact. If $\theta_e < \theta_e^{W=C}$, then a wetted contact is favored because it requires lower energy to wet the grooves. If $\theta_e > \theta_e^{W=C}$, then a composite contact is favored because it would take more energy to wet the grooves. The transition from a composite contact to a wetted contact occurs when the air pockets in the grooves are no longer thermodynamically stable and the liquid droplet begins to penetrate into the grooves. The existence of an energy barrier, however, may keep the system to remain at its current state. During the transition, according to Ishino and Okumura,[29] the system may go through a "mushroom" state, which occurs as the liquid penetration front propagates and reaches the edges of the droplet, and the "nucleation" of liquid at the center of the drop bottom then makes the whole droplet shape like a mushroom. In certain cases when a droplet is placed on a hydrophilic surface, the penetration may not stop after the penetration front reaches the edges of the droplet; instead, it continues to spread beyond the droplet and form a liquid film or liquid filaments over the surface. This is named the sunny side up state, for which Wenzel's theory can no longer be applied. At this state, the new apparent equilibrium contact angle becomes

$$\cos\theta^S = f\cos\theta_e + (1-f) \tag{6}$$

2.2. Simulation Method. In this study, we construct a mercury−copper system where mercury is the liquid and copper is the substrate. Copper was used in the studies of dopant effects in a nanocrystalline material[30] and film controlled wetting of platinum.[31] Liquid mercury is examined in this study because it is a heavier liquid and has not been widely investigated as a liquid droplet on substrates. Moreover, it is a single atomic material which requires less intensive computational time. The structure and thermodynamic properties of expanded liquid mercury were examined using molecular simulations.[32] Here, we employ the LAMMPS Molecular Dynamics Simulator[33] to simulate mercury and copper interactions with Lennard−Jones 12-6 type potential considering only short-range pairwise interactions:

$$U_{ij}(r) = 4\varepsilon_{ij}\left[\left(\frac{\sigma_{ij}}{r}\right)^{12} - \left(\frac{\sigma_{ij}}{r}\right)^{6}\right] \tag{7}$$

where r is the distance between any two particles; ε_{ij} and σ_{ij} are the potential well depth and the collision diameter, respectively. Subscripts i and j are the indices to represent liquid and solid particles. For a mercury−copper system, the liquid−liquid (ll) interaction parameters are $\varepsilon_{ll} = 2.6453$ kcal/mol and $\sigma_{ll} = 2.61$; the solid−solid (ss) interaction parameters are ε_{ss} that range from 0.026453 to 2.6453 kcal/mol and $\sigma_{ss} = 2.34$.[30,32] The liquid−solid (ls) interaction parameters are obtained by using Lorentze−Berthelot mixing rules:[19]

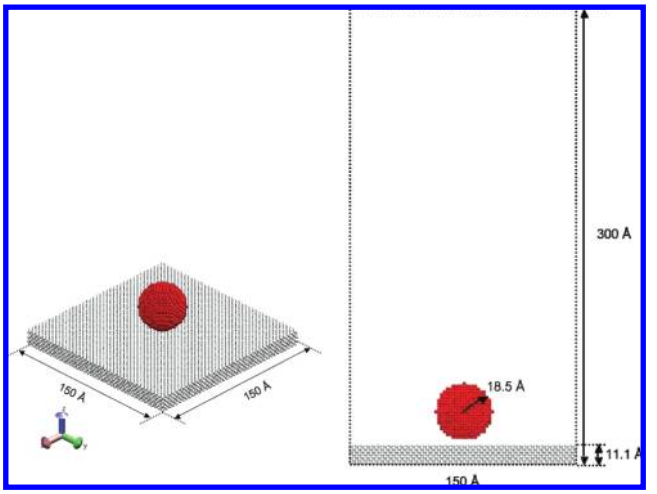

Figure 2. Initial configuration of a liquid droplet on a solid substrate: (left) perspective view and (right) side view with bounding box.

$$\sigma_{ls} = \sqrt{\sigma_{ll}\sigma_{ss}}, \quad \varepsilon_{ls} = \sqrt{\varepsilon_{ll}\varepsilon_{ss}} \tag{8}$$

The potential is truncated at a cutoff radius $r_c = 3.5\sigma_{ll}$.[34] We can further define the relative energy ε_r and relative size σ_r which are used to calibrate the affinity of a surface from hydrophilic to hydrophobic:[19,35]

$$\sigma_r = \frac{\sigma_{sl}}{\sigma_{ll}} = \sqrt{\frac{\sigma_{ss}}{\sigma_{ll}}}, \quad \varepsilon_r = \frac{\varepsilon_{sl}}{\varepsilon_{ll}} = \sqrt{\frac{\varepsilon_{ss}}{\varepsilon_{ll}}} \tag{9}$$

The details of the relationship between the relative energy and the resulting contact angle are described in section 2.5.

2.3. Simulation Models. The simulation model contains a mercury droplet with radius 18.5 Å placed above a copper substrate that comprises seven layers of 150 × 150 Å^2 copper atoms with a fcc-close-packed lattice and a lattice constant of 3.69 Å. The system consists of approximately 2000 mercury atoms (the volume of the droplet is about 45 nm^3) and 22 400 copper atoms for a substrate with a smooth surface and nearly 54 400 atoms for the largest grooved surface. The initial configuration of the system is shown in Figure 2.

The simulation box has lateral dimensions (x and y) that are equal to the dimensions of the substrate surface. The height of the simulation box (z) is twice as large as in the lateral dimension. The box has a size of approximately 150 × 150 × 300 Å^3. Periodic boundary conditions are set in the x and y directions, while the z direction is bounded with reflective walls to prevent the particles penetrating into the bottom of the substrate. A minimum image criterion is employed in the force calculations.[34]

The simulations are performed at constant number, volume, and temperature (NVT). Liquid atoms are assigned with random velocities according to Gaussian distribution. The liquid

(29) Ishino, C.; Okumura, K. *Eur. Phys. J. E* **2008**, *25*, 415–424.
(30) Millett, P. C.; Selvam, R. P.; Bansal, S.; Saxena, A. *Acta Mater.* **2005**, *53*, 3671–3678.
(31) Webb, E. B.III; Grest, G. S.; Heine, D. R. *Phys. Rev. Lett.* **2003**, *91*, 236102.
(32) Bomont, J.-M.; Delhommelle, J.; Bretonnet, J.-L. *J. Non-Cryst. Solids* **2007**, *353*, 3454–3458.
(33) Plimpton, S. *J. Comput. Phys.* **1995**, *117*, 1–19.
(34) Haile, J. *Molecular Dynamics Simulation*; Wiley-Interscience: New York, 1992.
(35) Nijimeijer, M.; Bruin, C.; Bakker, A.; van Leeuwen, J. *Phys. A* **1989**, *160*, 166–180.

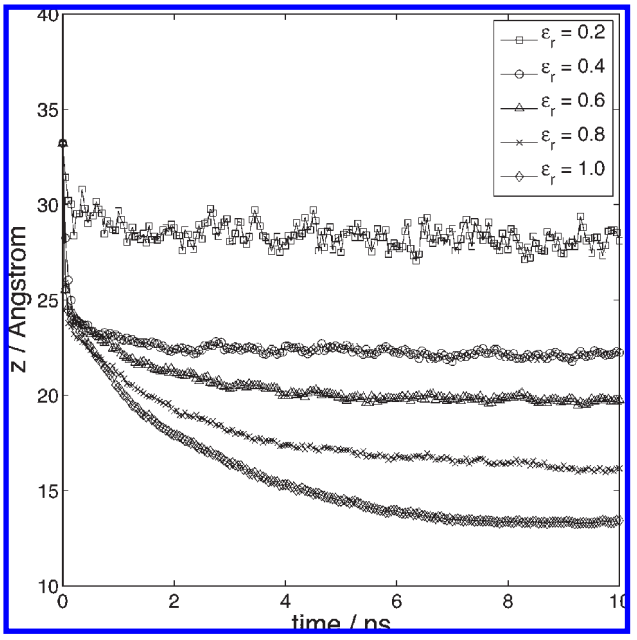

Figure 3. Trajectories of droplet centroid on a flat surface of systems with different relative energies.

velocities have a mean of 0.0 and are scaled to produce a desired temperature of 700 K. The solid velocities are initially set to zero. A Nosé−Hoover[36,37] temperature thermostat is applied every time step to maintain the temperature. The time step for Verlet integrator is chosen as 5 fs, and the neighbor list is updated every 10 time steps. The solid atoms are subjected to a constraint that zeros out all the forces applied to them in order to keep them fixed for the duration of the simulation. Doing so allows us to exclude the interactions between the solid atoms when building the neighbor list. It can reduce the computational time significantly.[35]

The equilibrium state of a system is determined based on examining the height of the droplet at its center of mass (centroid). The trajectories of the droplet centroid on a smooth surface with different relative surface energies are shown in Figure 3. The system configurations are recorded every 1 ns during equilibration and every 50 ps during production. For most simulations, it takes approximately 2−9 ns for a system to reach equilibrium depending on the surface energy. Typically, a total of 2×10^6 time steps (10 ns) is run to ensure that the system reaches equilibrium and it is then continued with 10^5 time steps (500 ps) for production. However, for some hydrophilic surfaces that have large roughness factors, the equilibration process can take up to 4×10^6 or even 6×10^6 time steps (20 or 30 ns).

2.4. Evaluation of Contact Angle. To obtain the contact angle from an equilibrated system, we evaluate the shape of the droplet by measuring the height and the radius of the droplet based on its geometric dimensions shown in Figure 4.

The contact angle can be estimated using the following geometric relationships:

$$\theta = 2tan^{-1}\left(\frac{h}{r'}\right) \text{ if } h < r \quad (10a)$$

$$\theta = 90^\circ + sin^{-1}\left(\frac{h-r}{r}\right) \text{ if } h > r \quad (10b)$$

Here, h and r are the height and the radius of the droplet, respectively; r' is the radius of the circular contacting interface

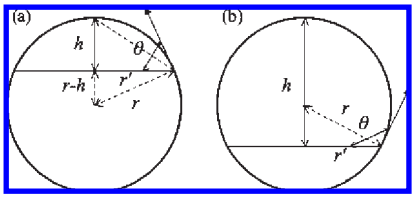

Figure 4. Evaluation of contact angle θ for (a) when the height of the droplet above the surface h is less than the radius r ($h < r$) and (b) when the height of the droplet above the surface h is larger than the radius r ($h > r$).

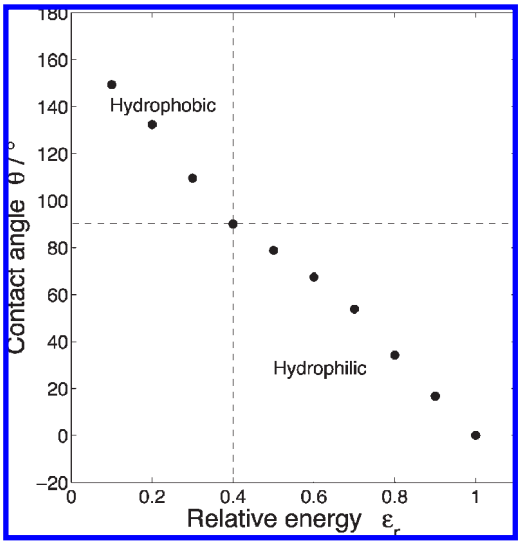

Figure 5. Contact angle (θ_e) versus relative energy parameter (ε_r) to calibrate surface affinities toward liquid.

area. If anisotropic spreading is expected, then measuring the contact angle from one plane is no longer sufficient. Therefore, three contact angles are considered to determine the degree of anisotropy in wetting: cylindrically averaged contact angle (θ_{avg}^{SIM}) which is calculated assuming the projected contacting area is a circle with a radius that is the average of the radius observed from each plane,[17] contact angle in the direction parallel to the grooves (yz plane) $\theta_{\parallel}^{SIM}$, and contact angle in the direction that is perpendicular to the grooves (xzplane) $\theta_{\perp}^{SIM}$.

2.5. Calibration of Surface Affinity for Liquid. In our studies, both hydrophobic and hydrophilic nanogrooved surfaces will be investigated. To vary a surface affinity for the liquid droplet from hydrophilic to hydrophobic, the relative energy ε_r that describes the attraction of the liquid to the solid surface needs to be adjusted accordingly. This parameter can be associated with properties of material such as the surface tension. As the attraction becomes weaker, that is, ε_r is small, the surface becomes more hydrophobic and leads to a larger contact angle. To calibrate the copper−mercury system, we vary the relative energy from 0.1 to 1. For each relative energy, the corresponding contact angle on a smooth surface is obtained (shown in Figure 5). The contact angle increases from 0° to 149° as ε_r decreases from 1.0 to 0.1. We obtain an intrinsically hydrophobic surface when $\varepsilon_r < 0.4$ and a hydrophilic surface when $\varepsilon_r > 0.4$.

3. Results and Discussions

Based on the models we described in section 2, we now study the wetting behavior of a droplet on a 1-D grooved surface at nanoscale. The grooves are defined by groove width a, height b,

(36) Nosé, S. *J. Chem. Phys.* **1984**, *81*, 511–519.
(37) Hoover, W. *Phys. Rev. A* **1985**, *31*, 1695–1697.

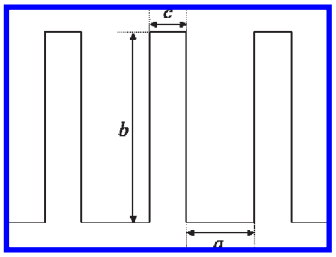

Figure 6. Schematic illustration of a substrate with grooved patterns. a denotes the groove width, b the groove height, and c the spacing between the grooves.

Table 1. Contact Angles Obtained from the Simulations for Different Roughness Factor r on a Hydrophobic Nanogrooved Surface with Surface Fraction $f = 0.5$[a]

r	$\theta_{\perp}^{SIM}$/°	$\theta_{\parallel}^{SIM}$/°	θ_{avg}^{SIM}/°	θ^{W}/°	θ^{C}/°	$\theta_{e}^{W=C}$/°
1.25	119.6	115.4	117.5^{W}	114.7	131.8	131.8
1.5	121.1	118.9	120.0^{W}	120.1	131.8	120.0
1.75	126.2	126.2	126.2^{W}	125.7	131.8	113.6
2.0	131.5	128.6	130.0^{C}	131.9	131.8	109.5
2.5	131.5	131.5	131.5^{C}	146.6	131.8	104.5
3.0	128.9	128.9	128.9^{C}	> 180	131.8	101.5
3.5	132.1	129.2	130.6^{C}	> 180	131.8	99.6
4.0	130.3	130.3	130.3^{C}	> 180	131.8	98.2

[a] Intrinsic contact angle θ_e on a flat surface is $\theta_e = 109.5°$.

and spacing c, as shown schematically in Figure 6. A series of roughness factor r and surface fraction f are examined. The resulting contact angles are compared with values obtained from Wenzel's and Cassie's theories. The study is performed for both hydrophobic surface ($\varepsilon_r = 0.3$) and hydrophilic surface ($\varepsilon_r = 0.5$) where the intrinsic affinities of these surfaces to liquid are obtained from the calibration study in section 2.5.

3.1. Hydrophobic Surface ($\varepsilon_r = 0.3$). *Contact Angle versus Roughness Factor*. An intrinsic hydrophobic surface can be obtained by adjusting the relative energy to be 0.3, which yields a contact angle of 109.5° on a smooth surface based on the calibration study shown in Figure 5. In this series of simulations, the effect of the roughness factor r on contact angle θ is studied. This is done by varying the groove height b from 1.85 to 23.77 Å, thereby obtaining the roughness factor to be ranging approximately from 1.25 to 4.0. The surface fraction is fixed to be $f = 0.5$ (by fixing the groove width, a, and the spacing between the grooves, c, both as 7.38 Å). The wetting behavior of this nanoscale system is expected to be different from a presumably larger, microliter droplet because of the sizes of the droplet and patterns. The contact angles obtained in all directions ($\theta_{\perp}^{SIM}$, $\theta_{\parallel}^{SIM}$, θ_{avg}^{SIM}) are calculated from the simulation results, listed in Table 1. The values from the cylindrical average θ_{avg}^{SIM} are compared with the values predicted from Wenzel's theory (θ^{W}) and Cassie's theory (θ^{C}), which are also listed in the table. For each value listed under θ_{avg}^{SIM}, we indicate the type of contact we observe at this particular contact angle: Wenzel (W) for wetted contact or Cassie (C) for composite contact. A theoretical prediction of the contact state is to compare the contact angle at the equilibrium state with the critical angle in eq 5. If the intrinsic contact angle on a smooth surface θ_e is larger than $\theta_e^{W=C}$, a composite contact is predicted. On the other hand, if θ_e is smaller than $\theta_e^{W=C}$, a wetted contact is predicted. Once the system reaches an equilibrium state, we compare our obtained contact angle with its corresponding theoretical Cassie's or Wenzel's contact angles depending the observed contact state.

Figure 7 shows the cylindrically averaged contact angle θ_{avg}^{SIM} as a function of the roughness factor. This relationship is

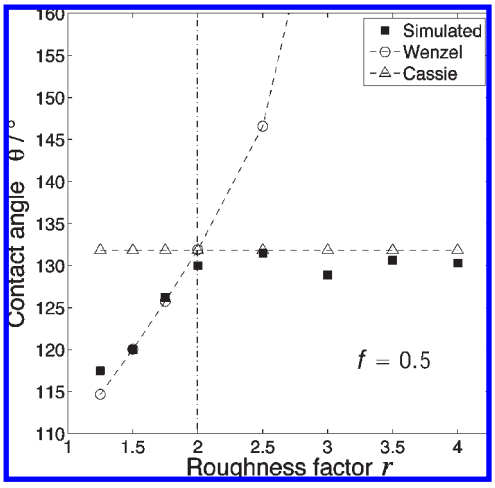

Figure 7. Contact angle θ versus roughness factor r for $f = 0.5$ on a hydrophobic nanogrooved surface and comparison with Wenzel's and Cassie's theories.

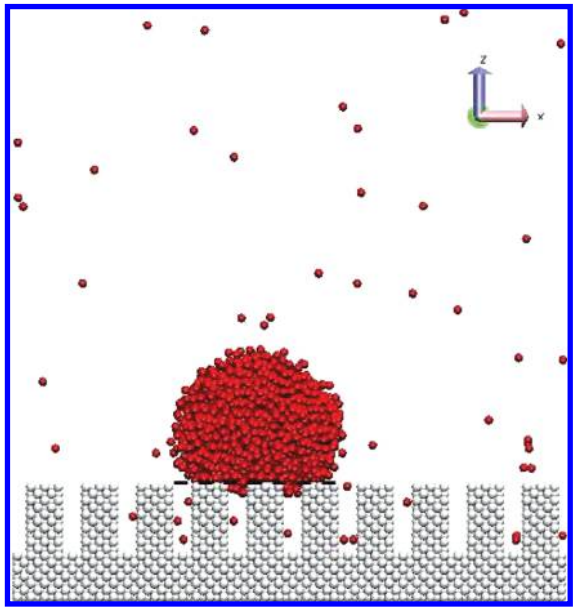

Figure 8. Partial wetting of a composite contact on a hydrophobic surface ($f = 0.5$, $r \approx 3.5$, $\theta = 130.6°$) where a small amount of liquid penetrates into the grooves (see below the dotted line).

compared with Wenzel's and Cassie's theories. It is clearly shown that when the roughness factor r is small ($r < 2.0$), the liquid can easily wet the grooves, and therefore, wetted contact is observed. As the roughness factor or groove height increases, the contact angle also increases, which is in good agreement with Wenzel's theory. As r reaches 2.0, composite contacts are observed and the contact angles remain approximately unchanged based on the roughness factor because it is energetically too costly to wet the grooves. This result also agrees well with Cassie's prediction for composite contacts. However, slight deviations are found in the composite regime where the theoretical Cassie's predictions overestimate the simulated values. This is because we found small amount of liquid atoms penetrating into the grooves, which makes a composite contact "partially" wetted, as shown in Figure 8. The original Cassie's theory assumes the composite surface is composed of solid and air, and it does not take into account this partial wetting.

The anisotropic liquid spreading can be quantified by comparing the contact angles obtained from the perpendicular

Table 2. Contact Angles Obtained from the Simulations for Different Surface Fraction f on a Hydrophobic Nanogrooved Surface with Roughness Factor $r \approx 2.0$[a]

f	$\theta_{\perp}^{SIM}$/°	$\theta_{\parallel}^{SIM}$/°	θ_{avg}^{SIM}/°	θ^{W}/°	θ^{C}/°	$\theta_{e}^{W=C}$/°
0.1	141.3	122.0	130.5^{W}	131.9	159.0	118.3
0.2	143.9	121.1	131.0^{W}	131.9	150.1	116.4
0.3	137.8	125.2	131.0^{W}	131.9	143.1	114.3
0.4	136.2	129.7	132.8^{W}	131.9	137.2	112.0
0.5	130.9	127.9	129.4^{W}	131.9	131.8	109.5
0.6	127.9	125.2	126.5^{C}	131.9	126.9	106.6
0.7	124.5	122.0	123.2^{C}	131.9	122.3	103.3
0.8	119.6	117.3	118.4^{C}	131.9	117.8	99.6

[a] Intrinsic contact angle θ_e on a flat surface is $\theta_e = 109.5°$.

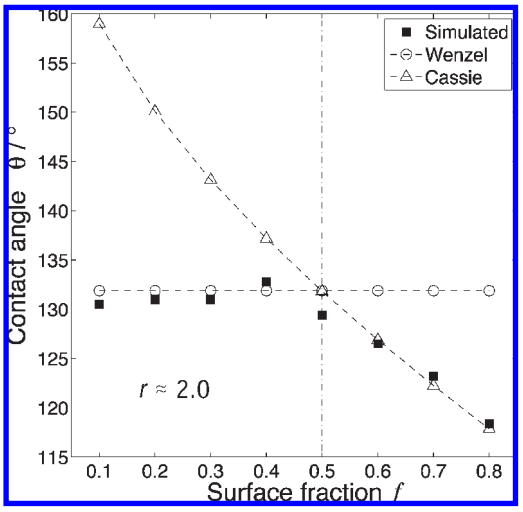

Figure 9. Contact angle θ versus surface fraction f for $r \approx 2.0$ on a hydrophobic nanogrooved surface and comparison with Wenzel's and Cassie's theories.

and parallel directions $\theta_{\perp}^{SIM}$ and $\theta_{\parallel}^{SIM}$, respectively. In the wetted contact regime, it is easier for the liquid to move in the direction that is parallel to the grooves and more constrained to move in the perpendicular direction, which results in $\theta_{\perp}^{SIM} > \theta_{\parallel}^{SIM}$. However, in this study, the difference between them remains $< 4°$ and is hardly noticeable.

Contact Angle versus Surface Fraction. To study the effect of the surface fraction (the fraction of the solid on the interface) on the contact angle, we vary the ratio of groove width and groove spacing (a/c) from 0.1 to 0.8 while maintaining the sum of these two values, that is, the projected length of the patterned substrate. This study is performed for two roughness factors: $r \approx 2.0$ and $r \approx 3.5$. The goal is to identify any differences induced by a combination of both roughness factor and surface fraction.

The results from the small roughness factor $r \approx 2.0$ are listed in Table 2. The contact angle as a function of the surface fraction is shown in Figure 9.

For the wide range of surface fraction studied, the contact angles in both wetted and composite contact regimes are consistent with theoretical predictions from Wenzel's and Cassie's theories. The transition from a wetted contact to a composite contact occurs at $f = 0.5$, which also agrees with the theoretical value.

In this study, the anisotropic liquid spreading is much more noticeable in wetted contacts. The difference between $\theta_{\perp}^{SIM}$ and $\theta_{\parallel}^{SIM}$ reaches as much as 22.8° when surface fraction is small, for example, $f = 0.2$. At this small fraction, it is much easier for the liquid to wet inside the grooves and induce more spreading in the direction that is parallel to the grooves. This anisotropic spreading behavior is a result of contact line pinning. It slows down the liquid to spread in the direction that is perpendicular to the grooves. Another effect of contact line pinning is the energy barrier for the liquid drop to undergo transition from Cassie to Wenzel contacts.[38,39] However, at the nanoscale, this might not be noticeable.[38] Snapshots of the system configuration from two different plane views are shown in Figure 10.

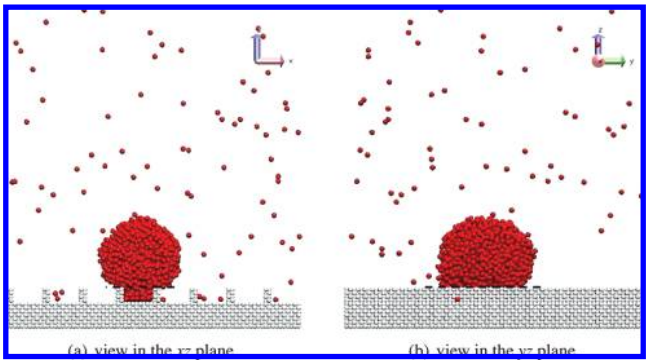

Figure 10. Anisotropic spreading of the liquid droplet observed by different plane views for wetted contact on a hydrophobic surface ($f = 0.1$, $r \approx 2.0$, $\theta_{\perp}^{SIM} - \theta_{\parallel}^{SIM} \approx 19.3$).

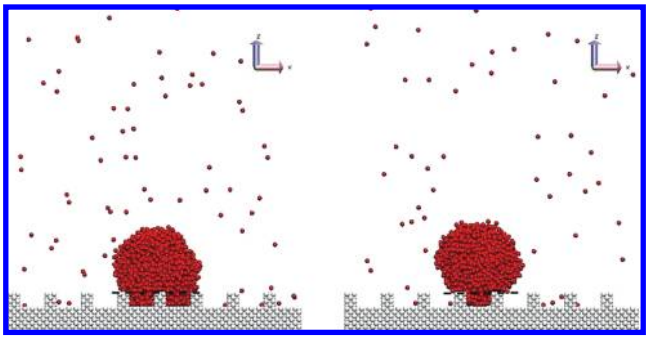

Figure 11. Droplet with wetted contact on a hydrophobic surface may result in two equilibrated configurations: (left) liquid wets two grooves and (right) liquid wets one groove.

We observed an interesting phenomenon with wetted contacts, which is that the droplet occasionally wets two grooves instead of one, as shown in Figure 11. When it occurs, the contact angle is found to be much smaller from the Wenzel's predicted value due to the increase in the wetted area. This phenomenon suggests that there are metastable states which may result in different contact angles. Similar observations are also mentioned in the previous studies.[28,40] Cassie's and Wenzel's theories provide the predicted contact angles obtained at the ground state.[41] There are energy barriers between multiple equilibrium states which could prevent the system from reaching the ground state. As the liquid settles down on the substrate, if the equilibrium shape that corresponds to a metastable state is reached first, then the configuration remains at this metastable equilibrium state until a perturbation is applied to the system. Factors such as the initial position of the droplet, the relative size of droplet, and the nanostructure may have influences on the

(38) Kusumaatmaja, H.; Blow, M.; Dupuis, A.; Yeomans, J. *Europhys. Lett.* **2008**, *81*, 36003.
(39) Tuteja, A.; Choi, W.; Ma, M.; Mabry, J. M.; Mazzella, S. A.; Rutledge, G. C.; McKinley, G. H.; Cohen, R. E. *Science* **2007**, *318*, 1618.
(40) Bico, J.; Marzolin, C.; Quéré, D. *Europhys. Lett.* **1999**, *47*, 220–226.
(41) Chung, J. Y.; Youngblood, J. P.; Stafford, C. M. *Soft Mater* **2007**, *3*, 1163–1169.

Table 3. Contact Angles Obtained from the Simulations for Different Surface Fraction f on a Hydrophobic Nanogrooved Surface with Roughness Factor $r \approx 3.5$[a]

f	$\theta_{\perp}^{SIM}$/°	$\theta_{\parallel}^{SIM}$/°	θ_{avg}^{SIM}/°	θ^{W}/°	θ^{C}/°	$\theta_e^{W=C}$/°
0.1	140.5	133.4	136.8^{C}	>180	159.0	105.3
0.2	140.0	129.7	134.5^{C}	>180	150.1	104.0
0.3	138.3	134.7	136.5^{C}	>180	143.1	102.6
0.4	136.2	126.9	131.3^{C}	>180	137.2	101.2
0.5	134.6	128.6	131.5^{C}	>180	131.8	99.6
0.6	127.9	125.2	126.5^{C}	>180	126.9	97.9
0.7	123.6	121.1	122.3^{C}	>180	122.3	96.2
0.8	116.6	118.8	117.7^{C}	>180	117.8	94.2

[a] Intrinsic contact angle θ_e on a flat surface is $\theta_e = 109.5°$.

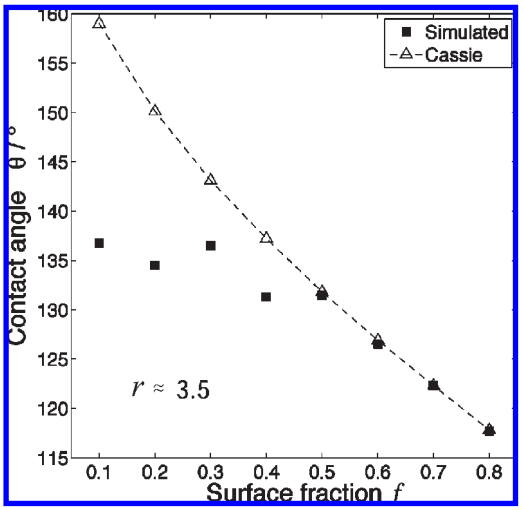

Figure 12. Contact angle θ versus surface fraction f for $r \approx 3.5$ on a hydrophobic nanogrooved surface and comparison with Cassie's theory.

final equilibrium shape and the resulting contact angle. Friction and line tension of the contact line are two main parts to form these energy barriers and are affected by substrate topological and chemical structure. The existence of metastable states leads to the contact angle hysteresis.

For a larger roughness factor, $r \approx 3.5$ (high groove height), only composite contact can be achieved because it is energetically too costly for the liquid droplet to wet the grooves completely. Our obtained contact angles are presented in Table 3. The contact angle as a function of surface fraction is also plotted in Figure 12 and compared with Cassie's theory.

The results show that when $f > 0.5$, the contact angles are consistent with Cassie's predictions; however, when $f < 0.5$, they deviate from Cassie's predictions. In the cases of $f < 0.5$, we again notice that there is a small amount of liquid penetration in the grooves. The amount of penetration varies with f as shown in Figure 13. When f is small, the groove width is large compared to the groove spacing, and a large amount of liquid atoms can easily penetrate into the grooves without completely wetting them (Figure 13a). Neither Cassie's or Wenzel's equation is valid in predicting this partially wetted case. For larger f, the amount of penetration is greatly reduced (Figure 13b). Therefore, the results are more consistent with Cassie's predictions.

Anisotropic liquid spreading is again observed (see Table 3). The difference of the contact angles in the parallel and perpendicular directions to the grooves ranges from 2.2 to 10.3°. When no liquid atoms are in the grooves, the droplet maintains its spherical shape (contact angle difference is <3°). However,

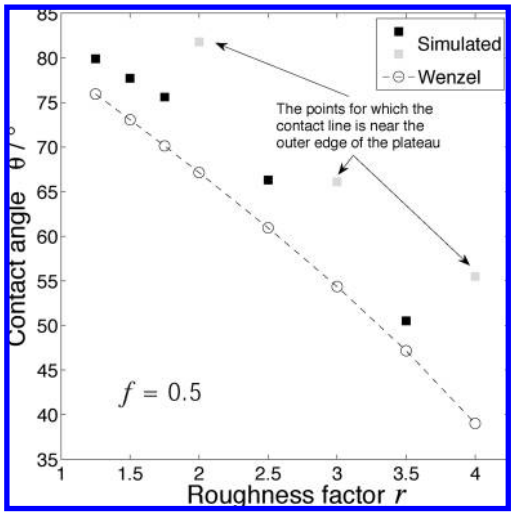

Figure 14. Contact angle θ versus roughness factor r for $f = 0.5$ on a hydrophilic nanogrooved surface and comparison with Wenzel's theory.

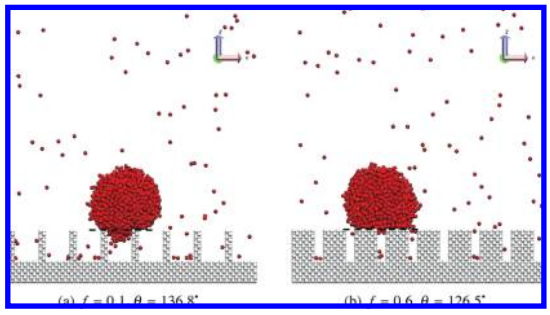

Figure 13. Small amount of liquid penetration is observed for a composite contact on a hydrophobic surface with $r \approx 3.5$. The amount is dependent on the surface fraction: (a) $f = 0.1$ and (b) $f = 0.6$.

when partial wetting occurs, the droplet spreads anistropically in the direction parallel to the grooves (contact angle difference reaches ≈10°). The more liquid atoms are in the grooves, the larger the anisotropy.

In summary, both Cassie's and Wenzel's theories are able to predict the contact angles rather accurately for a hydrophobic nanopatterned surface. However, at this scale, slight deviations are found when the surface patterns play a role in causing partial wetting, which then yield smaller contact angles than predicted. Anisotropic spreading is clearly observed, especially when partial wetting occurs.

3.2. Hydrophilic Surface ($\varepsilon_r = 0.5$). In this section, we focus our studies on nanoscale wetting behavior of droplets on hydrophilic surfaces. Similar to the hydrophobic surface studies, we will examine the contact angle changes with respect to roughness factor and surface fraction. An intrinsic hydrophilic surface can be obtained by adjusting the relative energy to be 0.5, which yields a contact angle of 78.8° on a smooth surface based on the calibration study shown in Figure 5. Since hydrophilic surfaces have an intrinsic contact angle of $\theta_e < 90°$ and the critical angle where a wetted contact transits into a composite contact $\theta_e^{W=C}$ is always larger than 90°, the theoretically predicted wetting behavior between the droplet and the substrate should always be wetted contacts. Therefore, for all the following wetting studies of hydrophilic surfaces, only Wenzel's predictions should be compared.

Table 4. Contact Angles Obtained from the Simulations for Different Roughness Factor r on a Hydrophilic Nanogrooved Surface with Surface Fraction $f = 0.5$[a]

r	$\theta_{\perp}^{SIM}/^{\circ}$	$\theta_{\parallel}^{SIM}/^{\circ}$	$\theta_{avg}^{SIM}/^{\circ}$	$\theta^{W}/^{\circ}$
1.25	81.0	78.9	79.9^{W}	75.9
1.5	80.8	74.5	77.7^{W}	73.1
1.75	79.3	71.9	75.6^{W}	70.1
2.0	84.5	79.1	81.8^{W}	67.1
2.5	68.0	64.6	66.3^{W}	60.9
3.0	79.2	54.3	66.1^{W}	54.4
3.5	52.6	48.4	50.5^{W}	47.2
4.0	56.1	54.9	55.5^{W}	39.0

[a] Intrinsic contact angle θ_e on a flat surface is $\theta_e = 78.8°$.

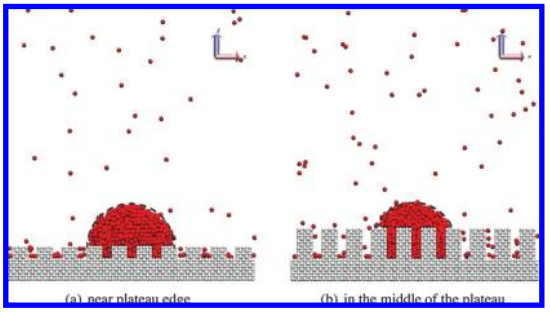

Figure 15. When (a) the three-phase contact line ends near plateau edges ($f = 0.5$, $r \approx 2.0$, $\theta = 81.8°$), the contact angles are not consistent with the predicted values, while they are when (b) the three-phase contact line ends in the middle of the plateaus ($f = 0.5$, $r \approx 3.5$, $\theta = 50.5°$).

Contact Angle versus Roughness Factor. The contact angles θ for different roughness factor r on a hydrophilic surface are shown in Figure 14, and a comprehensive list of data obtained is presented in Table 4.

Our results show that the relationship between the contact angle and the roughness factors r are qualitatively in agreement with Wenzel's predictions. The overall trend obeys Wenzel's theory which is that as roughness factor increases, that is, the groove gets deeper, more liquid atoms are found inside the grooves which results in a decrease in the contact angle. However, several of these data points tend to deviate from the theoretical values; they are identified and labeled in Figure 14. We found that these points correspond to when the position of the three-phase contact line between vapor, liquid, and solid is near the outer edge of the wetted plateau, as shown in Figure 15a. However, when the contact line is near the middle or the inner edge of the plateau (Figure 15b), the deviation is much smaller.

According to Lundgren et al.,[25] one of the reasons for the discrepancies is that, at the nanoscale, both Cassie's and Wenzel's theories do not take into account the effect of the sharp edges where the density of the solid atoms is particularly high. The influence of sharp edges in wetting was first discussed by Gibbs in the 1870s and was experimentally studied by Mason and colleagues in the late 1970s.[42] The effect of sharp edges can be considered as a part of contact angle hysteresis,[10,43,44] which is induced by the friction generated from the moving of the contact line. This friction is higher on a hydrophilic nonsmooth surface. For nanoscale wetting where the droplet size is comparable to the groove size, the local structure near the three-phase contact line becomes a major factor in influencing the wetting behavior. For a hydrophilic surface which has a strong liquid−solid interaction, this high local density exerts a strong constraint on the spreading of the droplet in the direction that is perpendicular to the grooves. Contact line pinning is observed when the constraints are taking place, which induces relatively larger contact angle than predicted. This constraint not only brings higher apparent contact angle but also induces more anisotropic liquid spreading. The largest difference between the contact angles in directions parallel and perpendicular to the grooves is found to be 24.9°. A snapshot of the anistropic spreading is shown in Figure 16.

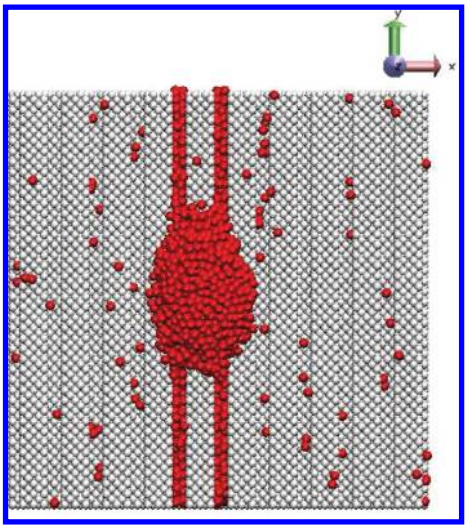

Figure 16. Anisotropic spreading along the direction parallel to the grooves (top view) of a wetted contact on a hydrophilic surface ($\varepsilon_r = 0.5, f = 0.5, r \approx 3.0, \theta_{\perp}^{SIM} - \theta_{\parallel}^{SIM} \approx 24.9$).

Table 5. Contact Angles Obtained from the Simulations for Different Surface Fraction f on a Hydrophilic Nanogrooved Surface with Roughness Factor $r \approx 2.0$[a]

f	$\theta_{\perp}^{SIM}/^{\circ}$	$\theta_{\parallel}^{SIM}/^{\circ}$	$\theta_{avg}^{SIM}/^{\circ}$	$\theta^{W}/^{\circ}$
0.1	94.0	76.2	85.0^{W}	67.1
0.2	93.8	77.9	85.7^{W}	67.1
0.3	89.3	76.8	83.0^{W}	67.1
0.4	87.9	72.6	80.1^{W}	67.1
0.5	83.1	70.5	76.7^{W}	67.1
0.6	81.2	73.2	77.2^{W}	67.1
0.7	78.8	76.5	77.6^{W}	67.1
0.8	76.5	75.4	75.9^{W}	67.1

[a] Intrinsic contact angle θ_e on a flat surface is $\theta_e = 78.8°$.

At this state, liquid droplet and liquid filaments filling the grooves coexist in the system. This is quite similar to the sunny side up state described in Ishino and Okumura.[29] In fact, the parallel contact angle we obtained has a fairly good agreement with the sunny side up state contact angle, which is the average of contact angle on the solid and "liquid" substrates, except when the surface fraction parameter is near 0 or 1.

Contact Angle versus Surface Fraction. We now study the effect of the surface fraction on contact angle on hydrophilic surfaces by fixing roughness factors. Again, two roughness factors $r \approx 2.0$ and $r \approx 3.5$ are examined. The results for when the roughness factor is small, that is, $r \approx 2.0$, are listed in Table 5 and shown in Figure 17.

The contact angles we obtained are significantly higher than Wenzel's predictions. We observed that, in this series of simulations, the three-phase contact lines of the droplet on the substrate are all near the outer edge of a plateau or even at the edge. Thus, the contact line pinning confines the droplet to

(42) Oliver, J.; Huh, C.; Mason, S. *J. Colloid Interface Sci.* **1977**, *59*, 568–581.
(43) Tadmor, R. *Langmuir* **2004**, *20*, 7659–7664.
(44) Kusumaatmaja, H.; Vrancken, R.; Bastiaansen, C.; Yeomans, J. *Langmuir* **2008**, *24*, 7299–7308.

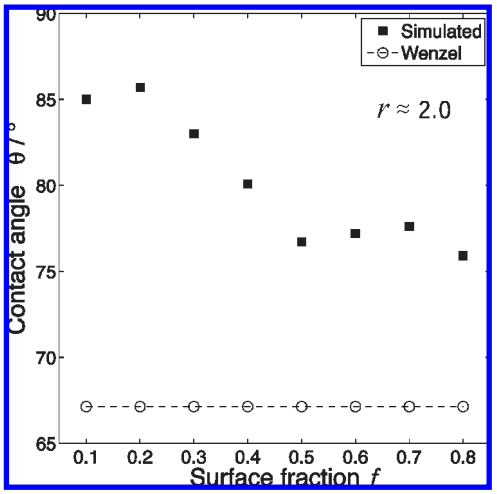

Figure 17. Contact angle θ veersus surface fraction f for $r \approx 2.0$ on a hydrophilic nanogrooved surface and comparison with Wenzel's theory.

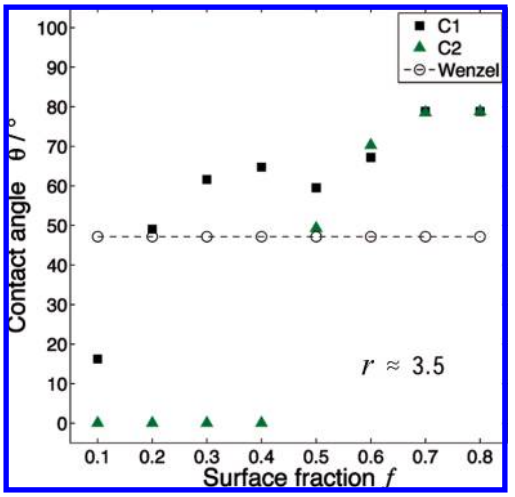

Figure 18. Contact angle θ versus surface fraction f for $r \approx 3.5$ on a hydrophilic nanogrooved surface with two initial configurations (C1 and C2) and comparison with Wenzel's theory.

Table 6. Contact Angles Obtained from the Simulations for Different Surface Fraction f on a Hydrophilic Nanogrooved Surface with Roughness Factor $r \approx 3.5$ Starting from Initial Configurations C1 and C2[a]

	C1				C2			
f	$\theta_{\perp}^{SIM}$/°	$\theta_{\parallel}^{SIM}$/°	θ_{avg}^{SIM}/°	θ^{W}/ °	$\theta_{\perp}^{SIM}$/°	$\theta_{\parallel}^{SIM}$/°	θ_{avg}^{SIM}/°	θ^{W}/ °
0.1	23.6	8.9	16.2^{W}	47.2	0	0	0^{W}	47.2
0.2	74.5	23.6	49.0^{W}	47.2	0	0	0^{W}	47.2
0.3	75.5	47.6	61.6^{W}	47.2	0	0	0^{W}	47.2
0.4	81.7	47.7	64.7^{W}	47.2	0	0	0^{W}	47.2
0.5	66.7	52.3	59.5^{W}	47.2	59.1	39.4	49.3^{W}	47.2
0.6	70.6	63.7	67.2^{W}	47.2	76.4	64.2	70.3^{W}	47.2
0.7	78.3	79.5	78.9^{W}	47.2	78.6	78.6	78.6^{W}	47.2
0.8	78.9	78.7	78.8^{W}	47.2	79.0	78.8	78.9^{W}	47.2

[a] Intrinsic contact angle θ_e on a flat surface is $\theta_e = 78.8°$.

spread out and yields a larger contact angle than predicted. This observation is consistent with the previous analysis for contact angle versus roughness factor study. As f goes to 1, the surface becomes a smooth surface, and the apparent contact angle approaches to the intrinsic contact angle on a smooth surface, which is $\theta_e = 78.8°$.

The results for roughness factor $r \approx 3.5$ are listed in Table 6 and shown in Figure 18. Since the grooves are relatively deep which generate a larger surface area, when surface fraction f is small, that is, $f < 0.4$, the hydrophilic grooves absorb a large portion of the liquid atoms into the grooves with a small amount of liquid remaining on the surface. At the equilibrium state, the apparent contact angles are found to be 0° in these cases. As discussed in the hydrophobic study, multiple equilibrium states can be identified depending on the system configuration. At the nanoscale, the initial position of the droplet and droplet size may also induce extra statistical error and larger random system fluctuation. To confirm this point for hydrophilic surfaces, we rerun the simulations with a different initial position by placing the droplet in between grooves. The two sets of simulations with different initial positions are labeled as C1 and C2 (C1 is where the droplet is placed above a groove, and C2 is above a plateau). The results show that the initial position, in fact, has an influence on which equilibrium state the system reaches first. As f increases, the contact line pinning starts to dominate, and the contact angles are higher than Wenzel's predictions. When f is near 1, the apparent contact angle approaches the contact angle on a smooth surface, 78.8°.

These series of results show that Wenzel's predictions for both roughness factor and the surface fraction are not accurate for a hydrophilic surface at the nanoscale. The contact angles are higher than predicted due to the contact line pinning near the plateau edges at nanoscale systems. The initial position of the droplet also plays an important role in the configuration of the equilibrium state.

4. Conclusions

In this study, we modeled and simulated droplets on nanogrooved surfaces to study the wetting properties of liquid at the nanoscale and examine the validity of Wenzel's and Cassie's theories at the nanoscale. We investigated both hydrophobic and hydrophilic surfaces with grooved patterns. The system used in this study consists of a mercury droplet and copper substrate.

For hydrophobic surfaces, our obtained contact angle as a function of the roughness factor with fixed surface fraction agreed quite well with Wenzel's and Cassie's theories for wetted and composite contacts, respectively. The transition from a composite contact to a wetted contact was also captured at the predicted critical contact angle. Similarly, the contact angle as a function of the surface fraction was also consistent with the theories when the roughness factor is small. However, when the roughness factor is large, partial wetting occurred in composite contacts, which induced deviations from Cassie's predictions. A small amount of liquid was found penetrating into the grooves. Therefore, Cassie's predictions are not quite accurate when partial wetting occurs at the nanoscale. For all hydrophobic surfaces, anisotropic wetting was found whenever wetting occurs, either totally wetted or partially wetted. This anisotropy was quantitatively measured. The level of anisotropy depended on the amount of liquid penetration into the grooves.

For hydrophilic surfaces, only wetted contacts were observed. Our results showed that, for contact angle versus roughness factor, the overall trend was consistent with Wenzel's theory. However, discrepancies were found when the three-phase contact line ended near plateau edges. For a nanosized droplet that has comparable size as the grooves, plateau edges have high local atomic density that can impose a strong constraint on the spreading of the liquid, which results in a higher contact angle than predicted. This contact line pinning should disappear when the droplet has a larger size compared to the grooves. Therefore, at the nanoscale, when the droplet size is comparable to or smaller than the groove size, the conventional Wenzel's theory would not be sufficient in accurately predicting the contacting angles.